Anisotropic self-diffusion of fluorinated poly(methacrylate) in metal–organic frameworks assessed with molecular dynamics simulation*

Tao Lu(鲁桃)[1], Biao Xu (徐彪)[1], Fei-Hong Ye(叶飞宏)[1], Xin-Hui Zhou(周馨慧)[3], Yun-Qing Lu(陆云清)[1,†], and Jin Wang(王瑾)[1,2,‡]

[1] School of Opto-Electronic Engineering, Nanjing University of Posts and Telecommunications, Nanjing 210023, China
[2] School of Telecommunication and Information Engineering, Nanjing University of Posts and Telecommunications, Nanjing 210023, China
[3] Key Laboratory for Organic Electronics and Information Displays & Institute of Advanced Materials, Nanjing University of Posts & Telecommunications, Nanjing 210023, China

(Received 7 August 2017; revised manuscript received 12 September 2017; published online 20 November 2017)

Utilizing the periodically structured metal–organic framework (MOF) as the reaction vessel is a promising technique to achieve the aligned polymer molecular chains, where the diffusion procedure of the polymer monomer inside MOF is one of the key mechanisms. To investigate the diffusion mechanism of fluorinated polymer monomers in MOFs, in this paper the molecular dynamics simulations combined with the density functional theory and the Monte Carlo method are used and the all-atom models of TFMA (trifluoroethyl methacrylate) monomer and two types of MOFs, $[Zn_2(BDC)_2(TED)]_n$ and $[Zn_2(BPDC)_2(TED)]_n$, are established. The diffusion behaviors of TFMA monomer in these two MOFs are simulated and the main influencing factors are analyzed. The obtained results are as follows. First, the electrostatic interactions between TFMA monomers and MOFs cause the monomers to concentrate in the MOF channel, which slows down the monomer diffusion. Second, the anisotropic shape of the one-dimensional MOF channel leads to different diffusion speeds of monomers in different directions. Third, MOF with a larger pore diameter due to a longer organic ligand, $[Zn_2(BPDC)_2(TED)]_n$ in this paper, facilitates the diffusion of monomers in the MOF channel. Finally, as the number of monomers increases, the self-diffusion coefficient is reduced by the steric effect.

Keywords: fluorinated polymer, metal–organic framework, self-diffusion coefficient, molecular dynamics

PACS: 31.15.at, 66.30.Fq, 61.46.–w **DOI:** 10.1088/1674-1056/26/12/123104

1. Introduction

Future optical transmission system and optical information processing technology require a large number of optical waveguide devices with novel functions, and these functions mainly rely on optical materials with high optical anisotropy.[1,2] Among many optical materials, the fluorinated polymer materials feature their low optical loss, low-cost fabrication and packaging,[3,4] but their optical anisotropies are generally weaker. For a given molecular structure of fluorinated polymers, this weak optical anisotropy is mainly caused by the disordered alignment of the polymer molecular chains. Therefore, it has become a hot research topic to improve the degree of orientation of polymer molecular chains, thereby improving the optical anisotropies of materials.[5–9]

Utilizing the periodically structured metal–organic framework (MOF) as a reaction vessel is a promising technique to achieve the aligned polymer molecular chains, in which involved are three major steps, namely, the adsorption of monomers into the pore channels of an MOF, the polymerization of the adsorbed monomers, which subsequently yields oriented polymer chains along the channels, and finally the removal of the MOF to obtain highly-oriented polymer materials.[10,11] Compared with other methods,[6–9] the method of using the nanoscale-confined space of MOF as a reactor for monomer polymerization can control the tacticity of the polymer chain at a molecular level.[12] The key mechanisms to improve the polymerization orientation of monomers include the efficient adsorption and diffusion of monomers in MOF. Therefore, in constructing optically anisotropic fluorinated polymers, fundamental considerations are to study the diffusion characteristics of fluorinated polymer monomers in MOF, and to explore the relationship between monomer tacticity and monomer diffusion properties.

In the present article, we investigate the diffusion behaviors of the TFMA (trifluoroethyl methacrylate), the monomer of PMATRIFE (polytetramethylacrylate), inside two MOFs, $[Zn_2(BDC)_2TED]_n$ (BDC = 1,4-benzenedicarboxylate, TED = triethylenediamine), and $[Zn_2(BPDC)_2TED]_n$(BPDC = 4,4′-biphenyldicarboxylate). Their all-atom models are established respectively by using molecular dynamics (MD) combined with the density-functional theory (DFT) and Monte Carlo (MC) method. Simulations are performed to study various factors influencing the diffusion behaviors of monomers in

*Project supported by the National Natural Science Foundation of China (Grant No. 61575096).
†Corresponding author. E-mail: jinwang@njupt.edu.cn
‡Corresponding author. E-mail: luyq@njupt.edu.cn
© 2017 Chinese Physical Society and IOP Publishing Ltd

MOF, which include the electrostatic interactions between the monomers and MOF, the anisotropic shape of the one-dimensional (1D) MOF channel, the length of the organic ligand, and the number of monomers inside the MOF.

2. Construction of TFMA monomer unit and all-atom MOF model

2.1. Construction and optimization of TFMA monomer unit

The initial structure of the TFMA monomer studied in this paper was obtained through the Cambridge Crystallographic Data Center (CCDC).[13] To ensure the rationality of the monomer unit in the MD simulation, it is necessary to perform the geometric optimization of the structural parameters of the initial TFMA monomer structure. In this paper, we used the software Material Studio to build and optimize the structure model. Parameters for geometric optimization were set as follows.[14] GGA\PBE was selected as the geometric optimization function; atom charge was selected for Mulliken analysis of charge distribution; and other parameters were set to be default values. The optimized molecular structure is shown in Fig. 1(a) and the energy curve during structural optimization is shown Fig. 1(b). Figure 1(b) shows that with the increase of optimization steps, the energy of the monomer decreases until it approaches to a minimum value. Vibration analysis was also performed on the optimized structure, and no imaginary frequency was found in the result, which indicates that the optimization has been completed.

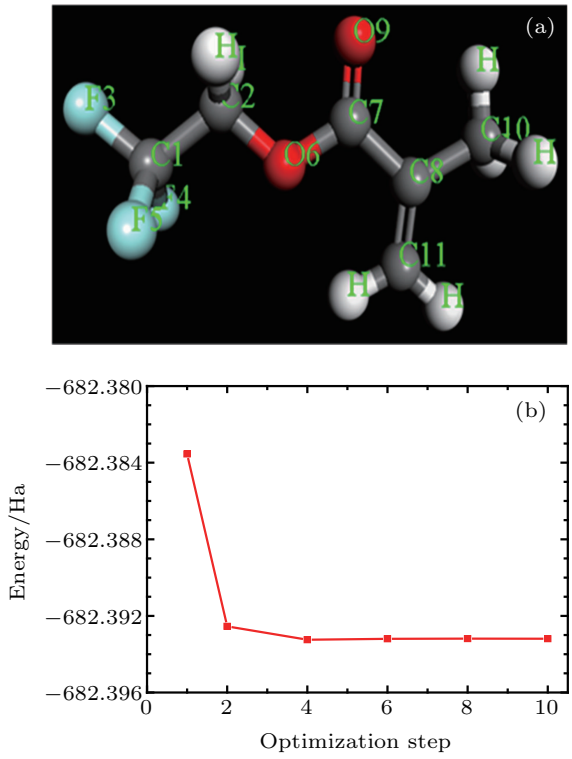


Fig. 1. (color online) (a) Optimized structure and (b) energy curve during structural optimization of the TFMA monomer.

2.2. Construction and optimization of MOF model

In the present article, the all-atom MOF models of $[Zn_2(BDC)_2(TED)]_n$ with atomic charge distribution, and $[Zn_2(BDC)_2TED]_n^{non-charge}$ without atomic charge distribution were established in order to study the effects of electrostatic interaction on the diffusion behaviors of TFMA monomers inside MOF. Also, to study the effects of the anisotropic shape of the 1D MOF channel, the all-atom model of $[Zn_2(BDC)_2TED]_n^{45°}$ (with the stable dihedral angle of BDC benzene ring rotated by 45°) was established. Further, to study the effects of the length of the organic ligand in MOFs on the diffusion behaviors of TFMA monomer, the all-atom model of $[Zn_2(BPDC)_2TED]_n$ was also established.

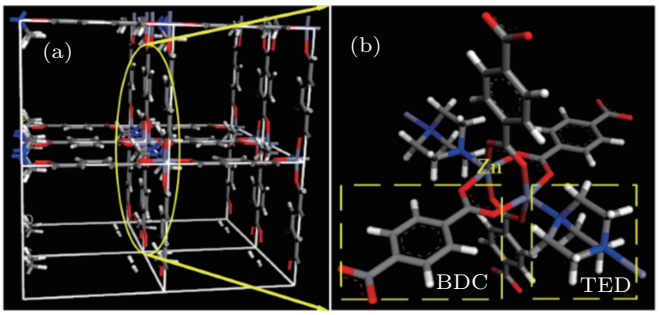


Fig. 2. (color online) (a) The optimized structural model and (b) the subunit of $[Zn_2(BDC)_2TED]_n$.

Considering the fact that the model constructions, optimizations, and diffusion simulation processes for these two MOFs, $Zn_2(BPDC)_2TED]_n$ and $[Zn_2(BDC)_2TED]_n$, are the same, $[Zn_2(BDC)_2TED]_n$ was taken below as an example to introduce these processes. The initial crystal structure of $[Zn_2(BDC)_2TED]_n$ used in this paper was also obtained from CCDC (CCDC-238860). Similarly, it was necessary to perform the geometric optimization of the initial structure model of $[Zn_2(BDC)_2TED]_n$ by using the DMol^3 quantum mechanics module, in which the DFT was employed. The specific parameters were set as follows: the GGA\PBE function was selected as the geometric optimization function, atomic charge was selected for the Mulliken analysis of charge distribution, and other parameters were set to be default values. The optimized structure model of $[Zn_2(BDC)_2TED]_n$ is shown in Fig. 2, and the energy curve of structural optimization is shown in Fig. 3. Figure 3 also shows that with the increase in optimization steps, the energy of the crystal structure $[Zn_2(BDC)_2TED]_n$ decreases until it approaches to a minimum value. Vibration analysis was performed on the optimized structure, and no imaginary frequency was found, which indicates that the optimization has been completed. The charge distribution of partial atom is shown in Table 1. Since only the organic ligand of $[Zn_2(BPDC)_2TED]_n$ is different from that of $[Zn_2(BDC)_2TED]_n$, the initial structural model of $[Zn_2(BPDC)_2TED]_n$ was obtained by replacing

BPDC in $[Zn_2(BPDC)_2TED]_n$ by the organic ligand BDC in $[Zn_2(BDC)_2TED]_n$, thereby modifying the lattice constant according to Ref. [15].

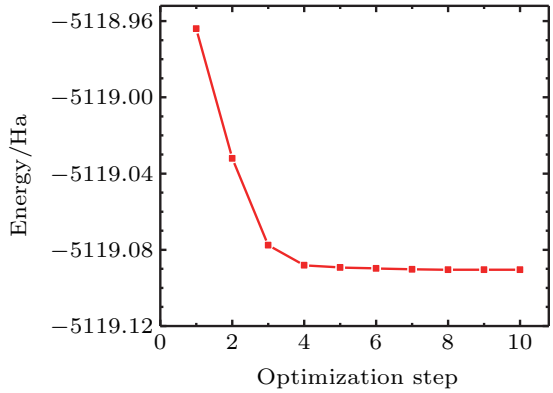


Fig. 3. (color online) Energy curve during structural optimization of the $[Zn_2(BDC)_2TED]_n$ model.

Table 1. Partial atomic charge distributions of the $[Zn_2(BDC)_2TED]_n$ model.

Atom	Charge/e	Atom	Charge/e
C1	–0.077	C29	–0.073
H2	0.167	O30	–0.546
Zn17	0.829	H31	0.116
N18	–0.543	C35	–0.073
C21	0.555	C36	–0.064
C26	–0.052	O40	–0.546
C28	–0.056	H54	0.114

The structural models of $[Zn_2(BDC)_2TED]_n^{non-charge}$, $[Zn_2(BDC)_2TED]_n^{45^\circ}$ and $[Zn_2(BPDC)_2TED]_n$ can be established on the basis of the $[Zn_2(BDC)_2TED]_n$ structure. The structural model of $[Zn_2(BDC)_2TED]_n^{non-charge}$ was obtained by selecting all atoms in the $[Zn_2(BDC)_2TED]_n$ structural model and modifying the charge of all atoms to zero. Since the structural model of $[Zn_2(BDC)_2TED]_n^{non-charge}$ was obtained by directly modifying the charge of the $[Zn_2(BDC)_2TED]_n$ structural model, the structure parameters of the two MOF models were identical, except for the difference in charge. The structural model of $[Zn_2(BDC)_2TED]_n^{45^\circ}$ can be obtained by rotating the dihedral angle of the benzene ring in the $[Zn_2(BDC)_2TED]_n$ structure by 45° as shown in Fig. 4(b). $[Zn_2(BPDC)_2TED]_n$ is shown in Fig. 5.

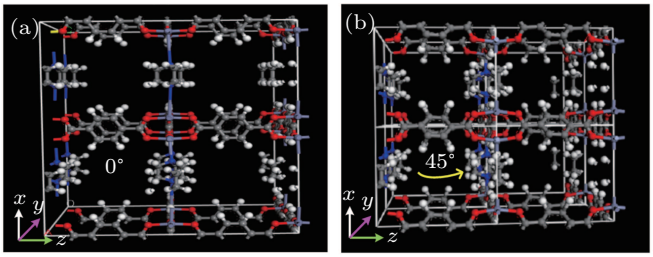


Fig. 4. (color online) (a) The structural model of $[Zn_2(BDC)_2TED]_n$, and (b) the structural model $[Zn_2(BDC)_2TED]_n^{45^\circ}$.

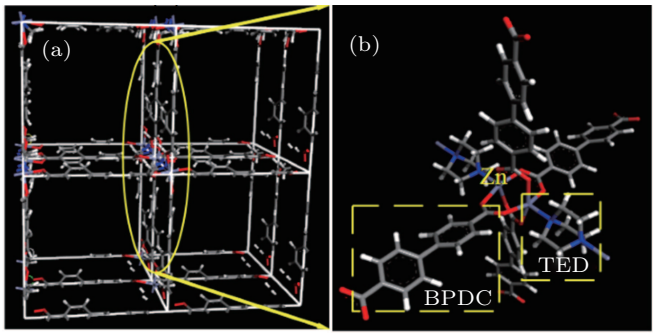


Fig. 5. (color online) (a) The optimized structural model and (b) the subunit of $[Zn_2(BPDC)_2TED]_n$.

3. Diffusion simulation of TFMA monomer in MOFs

3.1. Computational theory of the self-diffusion coefficient

The self-diffusion coefficient D_s in units of m^2/s can be calculated from the long-time behaviors of the mean-square displacement (MSD) of the atoms:[16,17]

$$D_s = \frac{1}{6}\lim_{t\to\infty}\frac{d}{dt}(\text{MSD}) = \frac{1}{6N}\lim_{t\to\infty}\frac{d}{dt}\left\langle\sum_{i=1}^{N}[r_i(t)-r_i(0)]^2\right\rangle, \quad (1)$$

where the subscripts denote different directions of particle diffusion, among which D_x and D_y are the self-diffusion coefficients along the x axis and the y axis, respectively (i.e., perpendicular to the channel direction), and D_z is the self-diffusion coefficient along the z axis (i.e., the channel direction); N denotes the number of particles diffused in the simulation; t is the simulation time; $r_i(t)$ is the displacement of the i-th particle at time t; $\langle\cdots\rangle$ denotes the ensemble average.

For porous materials, the calculation formula for the self-diffusion coefficient can be further simplified. When particles collide in porous materials, the transition scenario occurs due to the effect of the confined space. The diffusion state is reached only when the particles can escape from the regional restrictions and traverse the entire periodic lattice. With a long-time diffusion behavior, the MSD curve is bent to a different slope, which eventually reaches a stable diffusion state and forms a linear relationship with time. Therefore, the differential in Eq. (1) can be approximated with the slope of the MSD curve.

3.2. Simulation method and procedures

The simulation of the diffusion behaviors of the TFMA monomer was conducted in an MOF channel with 1×1×8 unit cells, among which 8 unit cells were in the direction of the MOF channel, and one unit cell was in the other two directions. The model is shown in Fig. 6. Before the diffusion simulation was carried out, the maximum adsorption number

of the TFMA monomer in $[Zn_2(BDC)_2TED]_n$ had been computed to be 2 per unit cell in the Sorption module of MS, in which the Monte Carlo method was employed. In the Sorption module, the calculation parameters were set as follows: the temperature was set to be 298 K, and the starting and ending pressures were chosen to be 0.1 kPa and 101 kPa, respectively. Afterwards, we selected 16 randomly arranged TFMA monomers as the objects of diffusion simulation in the $1\times1\times8$ $[Zn_2(BDC)_2TED]_n$ channel. After the TFMA monomers were placed in the $[Zn_2(BDC)_2TED]_n$ channel, a geometric optimization for the whole systemic structure was performed. The steps for geometric optimization were the same as described above. Then, MD was carried out in the optimized structure model.

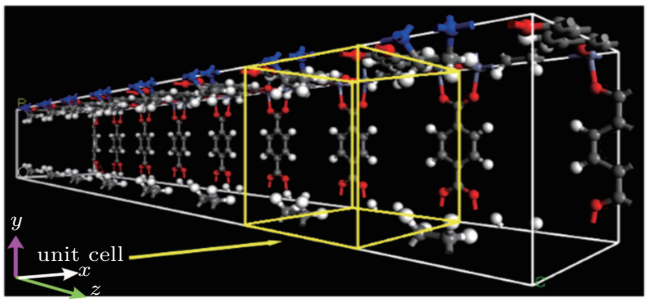


Fig. 6. (color online) Diagram of $[Zn_2(BDC)_2TED]_n$ model with $1\times1\times8$ unit cells.

The entire MD simulation was composed of three phases in the following order: a high-temperature relaxation, an annealing, and a data acquisition.[18,19] Taking into consideration the material properties of the MOF itself, the parameters for the high-temperature relaxation were as follows: NVT was selected as the ensemble; the temperature was set to be 1000 K; atom-based computation was used for intermolecular interaction potentials for both electrostatic force and van der Waals force. Other parameters remained unchanged. After the high-temperature relaxation phase, the structure was annealed to a target temperature of 343 K, which was an experimental temperature of the polymerization. Then, the MD was carried out for the annealed systemic structure with TFMA monomers in the $[Zn_2(BDC)_2TED]_n$ channel. In this phase, the MD simulation with the NVT ensemble was conducted for 100 ps. The total simulation steps were set to be 10^5, and the step length was 1 fs. Both the electrostatic force and the van der Waals force were atom based, while the other parameters remained unchanged. After the MD simulation, this all-atom systemic structure reached an equilibrated state as shown in Fig. 7, and therefore the diffusion behaviors of the TFMA monomer in $[Zn_2(BDC)_2TED]_n$ can be studied.

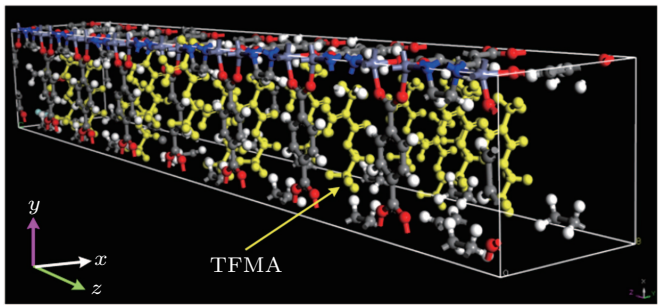


Fig. 7. (color online) Systemic structure model of $[Zn_2(BDC)2TED]_n$ containing 16 TFMA monomers after MD.

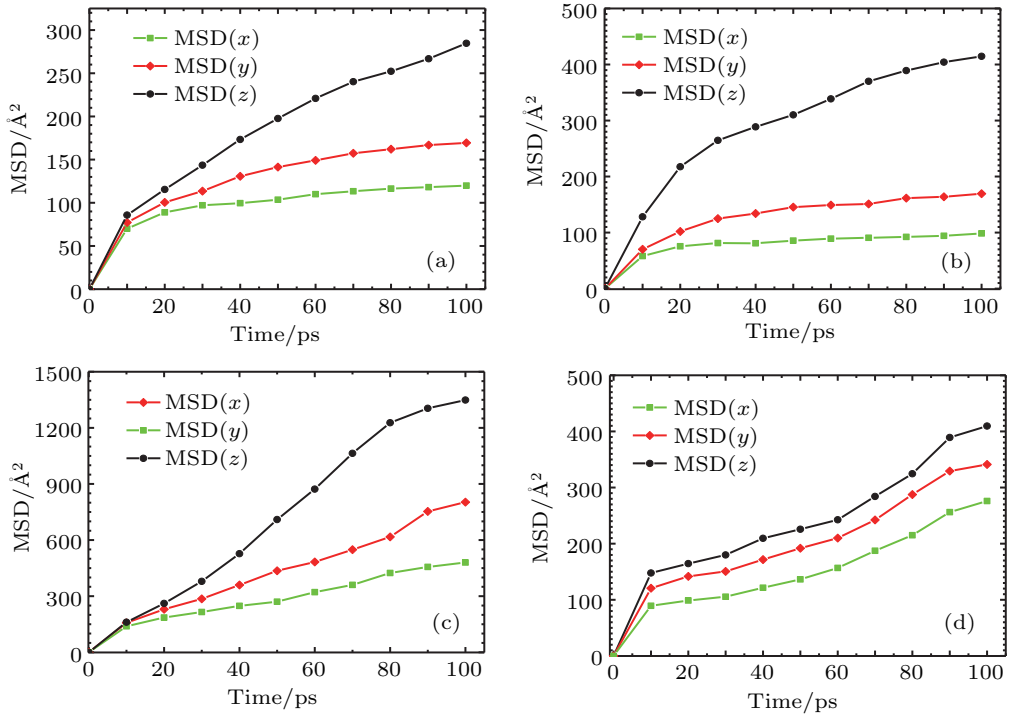


Fig. 8. (color online) MSD curves of TFMA monomers diffusing in different directions for (a) $[Zn_2(BDC)_2TED]_n$, (b) $[Zn_2(BDC)_2TED]_n^{non-charge}$, (c) $[Zn_2(BPDC)_2TED]_n$, and (d) $[Zn_2(BDC)_2TED]_n^{45^\circ}$.

The mean-square displacement curves of the TFMA monomers in $(Zn_2(BDC)_2TED]_n$, $(Zn_2(BDC)_2TED]_n^{non-charge}$, $[Zn_2(BPDC)_2TED]_n$, and $[Zn_2(BDC)_2TED]_n^{45^\circ}$ are shown in Figs. 8(a)–8(d), respectively. The MSD values in these figures are the average values among 16 TFMA monomers. It is worth noting that the diffusion reaches an equilibrium state when the MSD in all directions meet the condition that the slope between log(MSD) and $\log(t)$ is close to 1,[20] while the diffusion is unstable at the beginning of the MD simulation. With these figures, the self-diffusion coefficients of TFMA monomers in different MOFs were calculated according to Eq. (1) and are shown in Table 2. As explained above, the differential of Eq. (1) is approximated with the slope of the MSD curve between 80 ps and 100 ps. Table 2 also shows that there was a difference in the order of magnitude between D_z and D_x (D_y) values, which indicates the anisotropic behavior of TFMA monomers diffusing along the z-axis and the x axis (y axis). The anisotropy of D_s is consistent with that of a benzene molecule as measured by nuclear magnetic resonance (NMR) in the pore channel of $[Zn_2(BDC)_2TED]_n$.[20]

Table 2. Self-diffusion coefficients of TFMA monomer in different MOFs.

MOFs	$D_s/10^{-10}$ m^2·s^{-1}	
	Average of D_x and D_y	D_z
$[Zn_2(BDC)_2TED]_n$	0.03354	6.248
$[Zn_2(BDC)_2TED]_n^{non-charge}$	0.06812	12.409
$[Zn_2(BPDC)_2TED]_n$	0.03936	7.1564
$[Zn_2(BDC)_2TED]_n^{45^\circ}$	1.3641	1.9541

4. Analysis and conclusion

Based on the above simulation results, four factors influencing the diffusion of the TFMA monomer in MOF can be derived.

(i) **Interaction of the electrostatic force between fluorinated polymer monomer and MOF**

Table 2 shows that the self-diffusion coefficients of the trifluoroethyl methacrylate monomer in three directions of $[Zn_2(BDC)_2TED]_n^{non-charge}$ without atomic charge distribution are almost twice those of $[Zn_2(BDC)_2TED]_n$ with charge distribution. This diffusion behavior of TFMA monomers is caused by the interaction of electrostatic forces between monomers and MOFs. The channel wall of MOFs is a polar surface composed of metal ions and organic ligands. The electrostatic interaction between the polar channel walls of MOFs and the polar monomers reduces the gap between monomers, and the monomers become more concentrated inside MOFs, which slows down the monomer diffusion speed to a certain extent. In fact, we have also studied the diffusion behaviors of MMA monomers in $[Zn_2(BDC)_2TED]_n$ and $[Zn_2(BDC)_2TED]_n^{non-charge}$. The self-diffusion coefficient D_z of the MMA monomers in $[Zn_2(BDC)_2TED]_n$ is 4.932×10^{-10} m^2·s^{-1} and the average of D_x and D_y is 2.315×10^{-12} m^2·s^{-1}. These values are basically consistent with results in Ref. [20]. By comparing the self-diffusion coefficients of the TFMA and MMA monomers in $[Zn_2(BDC)_2TED]_n$ and $[Zn_2(BDC)_2TED]_n^{non-charge}$, we find that the electrostatic interaction between the TFMA monomers and MOFs is less than that between the MMA monomers and MOFs.

(ii) **Anisotropic shape of the 1D MOF channel**

By comparing self-diffusion coefficients of the TFMA monomers in $[Zn_2(BDC)_2TED]_n$ and $[Zn_2(BDC)_2TED]_n^{45^\circ}$, the dihedral angles of BDC benzene ring was rotated by 45°, it can be seen that in the $[Zn_2(BDC)_2TED]_n$, the diffusion coefficient D_z along the z axis was two orders of magnitude higher than the D_x (D_y) interchannel diffusion coefficient. This qualitatively indicates the anisotropic diffusion behavior of the TFMA monomers. However, the D_s values of the modified framework $[Zn_2(BDC)_2TED]_n^{45^\circ}$ are nearly isotropic. This is because in the case of a planar ligand where the dihedral angle of the BDC benzene ring is almost 0°, the TFMA monomers rarely diffuse across the channel (x, y axes), but diffuse only along the channel direction (z axis). Whereas in the case of a non-planar ligand where the dihedral angle of the BDC benzene ring is almost 45°, the TFMA monomers diffuse not only in the channel direction, but also through channels perpendicular to the channel direction.

(iii) **Ligand lengths of MOFs**

The comparison between self-diffusion coefficients of the TFMA monomer in $[Zn_2(BDC)_2TED]_n$ and $[Zn_2(BPDC)_2TED]_n$ shows that in $[Zn_2(BDC)_2TED]_n$ with a slightly shorter BDC ligand, the self-diffusion coefficients of the TFMA monomer are a bit smaller. This is because the shorter organic ligand BDC results in smaller MOF channels, which restricts the free rotation of monomers, thereby affecting the diffusion of monomers. In the other case, the longer organic ligand BPDC results in larger MOF channels, which facilitates the diffusion of TFMA monomers in the channel.

(iv) **Number of monomers diffusing in MOFs**

Furthermore, the diffusion procedures of the TFMA monomers with different total numbers of monomers inside $[Zn_2(BDC)_2TED]_n$ were simulated and respective diffusion coefficients were calculated, as shown in Fig. 9(a). It should be noted that the maximum absorption number of TFMA monomers in $[Zn_2(BDC)_2TED]_n$ is 2 per unit cell, therefore the maximum number of TFMA monomers inside our $1\times1\times8$ MOF channel is 16. The results show that the self-diffusion coefficient decreases with the increase of the total number of the monomers. This behavior is caused by the steric effect among monomers,[21] which plays a role

for a large total number of monomers inside MOF. In the case of MMA monomer, we also studied influence of the total number of monomers inside MOF. The maximum absorption number of MMA monomers in $Zn_2(BDC)_2TED]_n$ is 2.75 per unit cell, and 22 inside our $1 \times 1 \times 8$ MOF channel. The respective diffusion coefficients for different numbers of MMA monomers in $[Zn_2(BDC)_2TED]_n$ were calculated and are shown in Fig. 9(b). The similar behaviors, in which the self-diffusion coefficient decreases with the increase of the total number of the monomers, can be seen. This result further confirms the influence of the number of monomers on its diffusion characteristics.

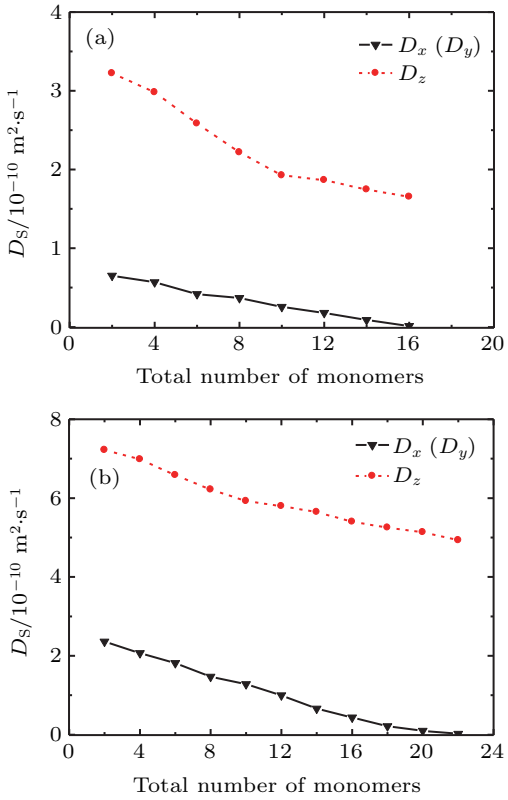


Fig. 9. (color online) (a) Self-diffusion coefficients of the TFMA monomer with different numbers of molecules in $[Zn_2(BDC)_2TED]_n$. (b) Self-diffusion coefficients of the MMA monomer with different numbers of molecules in $[Zn_2(BDC)_2TED]_n$.

By utilizing the MD combined with DFT and MC, we performed simulations to investigate the diffusion behaviors of the TFMA monomers in $[Zn_2(BDC)_2TED]_n$, $[Zn_2(BDC)_2TED]_n^{non-charge}$, $[Zn_2(BDC)_2TED]_n^{45^\circ}$, and $[Zn_2(BPDC)_2TED]_n$. We verified the anisotropic diffusion behaviors of the TFMA monomers in MOFs, and explored four factors influencing the diffusion behaviors of the TPMA monomers in MOFs.

The study of the influence of these four factors provides theoretical prediction methods of selecting the polymer monomers or MOFs,and controlling the orientation degree of polymer chains. These results are helpful in further investigating the effects of the absorption and diffusion behaviors of polymer monomers on the orientation of polymer chains in MOFs.

References

[1] Luo J and Lai Y 2014 *Sci. Rep.* 2014 **4** 5875
[2] Wu Q, Turpin J P and Werner D H 2012 *Light Sci. Appl.* **1** e38
[3] Bosc D, Maalouf A, Messaad K, et al. 2013 *Opt. Mater.* **35** 1207
[4] Oh M C, Chu W S, Shin J S, *et al*. 2016 *Opt. Commun.* **362** 3
[5] Thorkelsson K, Bai P and Xu T 2015 *Nano Today* **10** 48
[6] Dou L, Zheng Y, Shen X, Wu G, Fields K, Hsu W C, Zhou H, Yang Y and Wudl F 2014 *Science* **343** 272
[7] Stupp S I and Palmer L C 2013 *Chem. Mater.* **26** 507
[8] Yang J S, Huang D H, Cao Q L, Li Q, Wang L Z and Wang F H 2013 *Chin. Phys. B* **22** 098101
[9] Arakawa Y, Kuwahara H, Sakajiri K, Kang S, Tokita M and Konishi G I 2015 *Liquid Cryst.* **42** 1419
[10] Distefano G, Suzuki H, Tsujimoto M, *et al*. 2013 *Nat. Chem.* **5** 335
[11] Kaneti Y V, Tang J, Salunkhe R R, *et al*. 2017 *Adv. Mater.* **29**
[12] Uemura T, Nakanishi R, Kaseda T, *et al*. 2014 *Macromolecules* **47** 7321
[13] Groom C R and Allen F H 2014 *Angew. Chem. Int. Ed.* **53** 662
[14] Prakash M, Jobic H, Ramsahye N A, *et al*. 2015 *J. Phys. Chem. C* **119**
[15] Lee J Y, Pan L, Huang X, *et al*. 2011 *Adv. Funct. Mater.* **21** 993
[16] Ju Y Y, Zhang Q M, Gong Z Z and Ji G F 2013 *Chin. Phys. B* **22** 083101
[17] Skoulidas A I and Sholl D S 2005 *J. Phys. Chem. B* **109** 15760
[18] Imran M, Hussain F, Rashid M, *et al*. 2016 *Chin. Phys. B* **25** 076601
[19] Asad A and Jiang-Tao W 2011 *Chin. Phys. B* **20** 106601
[20] Takayanagi M, Pakhira S and Nagaoka M 2015 *J. Phys. Chem. C* **20** A47
[21] Ford D C, Dubbeldam D, Snurr R Q, *et al*. 2012 *J. Phys. Chem. Lett.* **3** 930